EVALUATION OF SPECTRAL EFFECT ON MODULE PERFORMANCE USING MODELED AVERAGE WAVELENGTH

Giorgio Belluardo[1*], Jochen Wagner[2], Anke Tetzlaff[2], David Moser[1]
[1]Institute for Renewable Energy, EURAC Research, Viale Druso 1, 39100 Bolzano (BZ), Italy
[2]Institute for Applied Remote Sensing, EURAC Research, Viale Druso 1, 39100 Bolzano (BZ), Italy

*Phone: +39 0471 055626; Fax: +39 0471 055699; E-mail: giorgio.belluardo@eurac.edu

ABSTRACT: Since solar cells are spectrally selective, photovoltaic modules are affected by the spectral distribution of the in-plane irradiation. This is in turn dependent on the radiative transfer through the atmosphere.
Many parameters are used to characterize the quality of spectral distribution, i.e. its balance towards low rather than high wavelengths. They are based on measured or modeled solar spectra, and may or not require the measurement of the module spectral response.
This paper presents a method for the evaluation of spectral effect through the use of the average wavelength of modeled spectra. It results therefore useful when no measured spectral data is available, and does not require the measurement of the module spectral response.
The integral value of modeled spectral distribution is first validated through comparison with measured irradiance. The average wavelength is then used to assess the spectral effect on the performance of different PV technologies installed at Airport Bolzano Dolomiti (ABD) test facility and monitored by EURAC: polycrystalline silicon (pc-Si), single junction amorphous silicon (a-Si), micromorph silicon (a-Si/µc-Si), Cadmium Telluride (CdTe) and Copper Indium Gallium Selenide (CIGS). Daily, seasonal and meteorology-related variability of the parameter is also assessed.
Keywords: spectral effect, average wavelength, modeled spectrum, performance

1 INTRODUCTION

Many parameters are used to characterize the quality of spectral distribution: average photon energy [1, 2], average wavelength, air mass [3], useful fraction [4], spectral mismatch correction [5]. They are based on measured or modeled solar spectra, and may or not require the measurement of the module spectral response.

The purpose of this work is to present the effect of solar spectrum on the performance of different PV technologies using a methodology that does not require availability of ground measurements of spectral irradiance. The spectral distribution is represented by a unique value, the average wavelength, which is calculated from modeled spectra using satellite retrieved cloud information. The integral value of spectral distribution is validated through comparison with measured irradiance. This work also analyses the variability of spectral distribution during the day, with seasons, under different meteorological conditions, and the effect of shading due to adjacent mountains.

2 METHODOLOGY

2.1 Modeling of solar spectrum

Spectrally resolved solar surface irradiance is calculated with the SPECMAGIC algorithm [6]. This algorithm allows for a quick provision of highly accurate data records because it uses lookup tables (LUTs), i.e. pre-computed radiative transfer model (RTM) results which contain the transmittance for a variety of atmospheric and surface states. In this way, RTM does not need to be resolved for every satellite pixel and time, but the transmittance can just be extracted from the LUTs by interpolation. Finally, solar surface irradiance can be calculated from the transmittance by multiplication with the extraterrestrial incoming solar flux density.

The following input parameters are taken into account:

- aerosol optical depth (from monthly climatologies)
- surface albedo (using land use maps)
- single scattering albedo (fixed value)
- total column ozone (fixed value)
- water vapor column (from monthly climatologies)
- Sun – Earth distance
- solar zenith and azimuth angle

In a first stage the direct and global clear sky spectral irradiance is calculated with the SPECMAGIC algorithm. In order to decrease the computation run-time the correlated-k approach of Kato et al. is used [7], which comes with 32 bands in the whole solar spectrum, each of which is characterized by a unique set of values of gaseous absorption coefficients. The component j of irradiance is derived as follows:

$$I_{j,mod}(\lambda) = I_{j,AM1.5}(\lambda)\frac{I_{j,mod}(k)}{I_{j,AM1.5}(k)}$$

where:

- $I_{j,AM1.5}(\lambda)$: irradiance of the standard spectrum at air mass 1.5
- $I_{j,mod}(k)$: irradiance modeled with SPECMAGIC, with resolution Kato
- $I_{j,AM1.5}(k)$: irradiance of the standard spectrum at air mass 1.5, with resolution Kato

The direct and global actual spectral irradiance is then obtained by attenuating the clear sky spectral irradiance according to the actual clouds using cloud index from MeteoSwiss [8]. The cloud index is converted to the clear sky index and direct and global irradiance are simply calculated as the product of clear sky irradiance and clear sky index. A height correction is also performed taking into account the site altitude and solar

zenith angle.

The modeled direct and global horizontal spectral irradiance are finally modified in order to take into account the shading of the surrounding mountains, and converted to tilted plane by applying a model which assumes an isotropic distribution of diffuse radiation and a fixed value of surface albedo.

2.2 Average wavelength index

The average wavelength of a solar spectrum is the wavelength for which the integral value of irradiance at lower wavelengths equals the integral value of irradiance at higher wavelengths. In other words, at the average wavelength the cumulative spectral irradiance is exactly half of the broadband irradiance.

The spectral range considered in this study is between 307 nm and 1965 nm (corresponding to Kato bands 4 to 27). This is done in order to consider the range of photovoltaic conversion of state of the art solar cells (about 300 nm to 1700 nm). The average wavelength values of the AM1.5 standard spectra in the abovementioned spectral range is 716 nm for direct irradiance and 699 nm for global irradiance.

3 EXPERIMENTAL SETUP

The photovoltaic technologies considered in this study are installed at the Airport Bolzano Dolomiti (ABD) test facility (46.45778 N, 11.32861 E), which has been connected to the medium-voltage grid in August 2010. The plant is composed of a commercial part of 662 kW with CdTe modules, and a 62 kW experimental part with 24 different types of modules, divided into 39 arrays ranging between 1 and 2 kW each, and mounted on fixed racks as well as on single- and dual axis trackers [9]. The technologies considered in this study have a fixed tilt of 30° and an azimuth angle of 8.5° West of South. The site elevation is 262 m above the sea level.

The production data is recorded by commercial inverters with a frequency of 15 minutes. The facility is also equipped with a meteo station for the measurement of horizontal (global and diffuse, secondary standard pyranometers) and global plane-of-array irradiance (secondary standard pyranometer), direct irradiance (secondary standard pyrheliometer), and wind speed (2-axis ultrasonic anemometer) with a frequency of 1 minutes. Measured data are then averaged on a 15-minutes time basis.

4 RESULTS AND DISCUSSION

4.1 Validation of modeled data

In a first stage, the integral values of spectral irradiance on both horizontal and tilted (30°) planes are calculated with SPECMAGIC considering the range between 250 and 3000 nm, which is slightly broader than the spectral sensitivity of the secondary standard pyranometers (285-2800 nm). However, this spectral mismatch results in a difference of just 0.04% of irradiance for the standard spectrum 1.5G, mainly concentrated in the long-wave region.

The modeled data is then validated against the corresponding measured values, for year 2011. Figure 1 shows a good agreement, especially for points corresponding to clear sky conditions (ratio of diffuse to global horizontal irradiance, *DtGHI,* lower than 0.20), on the horizontal plane (Fig. 1b). The comparison on tilted plane presents a lower agreement with respect to the horizontal plane, thus indicating a need for a further improvement of the model.

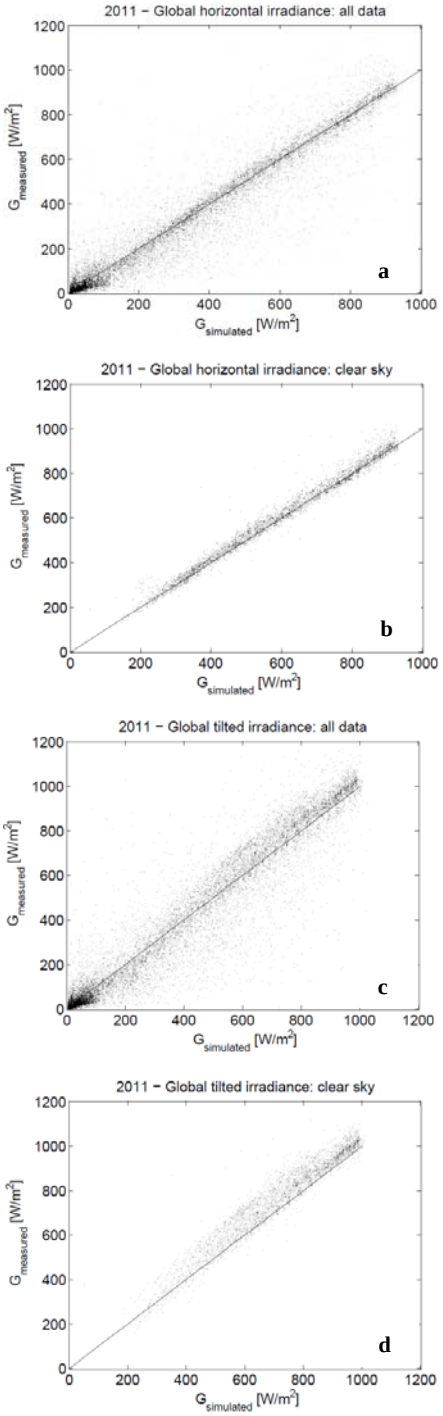

Figure 1: comparison of simulated and measured global irradiance at ABD test installation, year 2011. a) horizontal plane, unfiltered data (R^2=0.918) b) horizontal plane, clear sky conditions (R^2=0.981) c) tilted plane, unfiltered data (R^2=0.909) d) tilted plane, clear sky conditions (R^2=0.935)

Furthermore, a comparison between modeled and measured solar spectra data has to be carried out in order to increase the consistency of the model. This will be the object of a future study.

4.2 Site spectral characterization

In order to characterize the ABD site with respect to average wavelength, the variability of this index during the day and the year, and under the shading effect of mountains and cloud cover is analyzed.

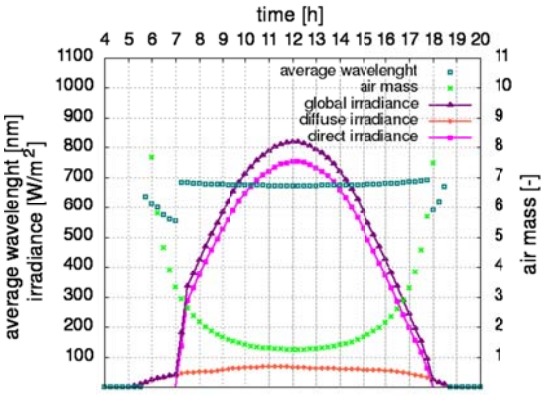

Figure 2: daily variation of average wavelength index over a clear sky day (28th August, 2011, *DtGHI* 0.11). Direct, diffuse and global irradiance are also shown (left y-axis), as well as air mass (right y-axis). All values refer to the horizontal plane

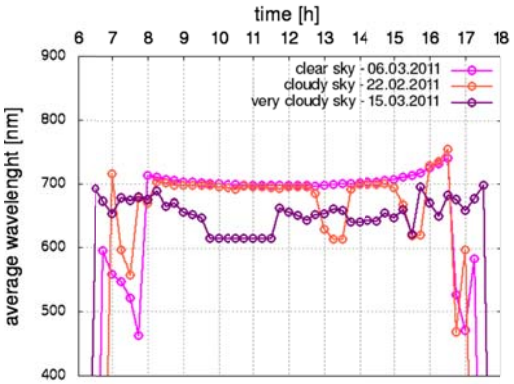

Figure 3: daily variation of average wavelength index due to cloud cover through comparison of a clear sky (*DtGHI* 0.11), cloudy sky (*DtGHI* 0.59) and very cloudy sky (*DtGHI* 0.98) day in 2011. Values refer to tilted plane (30°)

On the horizontal plane, in a clear sky summer day (Figure 2), after sunrise (5:45 AM) the surrounding mountains shade the site and only the diffuse irradiance is visible. The average wavelength is therefore shifted towards wavelengths typical of this component, i.e. towards blue wavelengths, the more the air mass decreases. As soon as the direct irradiance reaches the site (7:15 AM), there is a switch towards red wavelengths, due to the influence of the red-shifted direct component. From this moment on, the index does not vary significantly, even though a minimum point is reached at noon, corresponding to the lowest value of air mass and angle of incidence (AOI). As for sunrise, at sunset a blue-shift is clearly visible (mountain shading starts at approximately 6:00 PM).

Figure 3 shows the effect of meteorological conditions, basically cloud cover, over the index. Three days corresponding to clear sky conditions (DtGHI close to 0), cloudy sky conditions (DtGHI close to 0.50) and very cloudy sky conditions (DtGHI close to 1) are considered. It is clear that clouds produce instability on the value of average wavelength. The more the sky is covered, the more the direct irradiance component weakens and the index is shifted towards blue wavelengths.

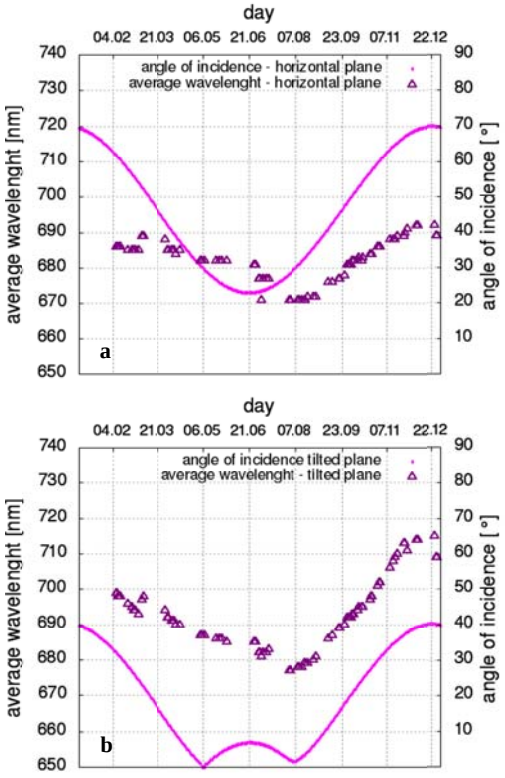

Figure 4: seasonal variation of average wavelength at around noon for year 2011, for a) horizontal and b) tilted (30°) plane, under clear sky conditions (*DtGHI* < 0.20). Corresponding angle of incidence is also displayed. Values for January are missing

The seasonal variation of average wavelength index is shown in Figure 4, both on the horizontal (Fig. 4a) and tilted plane (Fig. 4b). For each day only the value corresponding to the minimum of angle of incidence, that occurs at different times around noon depending on the season, has been considered and filtered for DtGHI less than 0.20 in order to minimize the variability due to cloud cover. Results show that the average wavelength index does not follow the trend of the corresponding angle of incidence for both horizontal and tilted plane, thus indicating that the geometric effect is not the only factor influencing this index. The average wavelength presents an oscillation between a minimum value around August and a maximum value occurring around winter solstice. One would expect a minimum at around summer solstice for the horizontal plane, and a second minimum around

the beginning of May for the tilted plane. Actually, the mismatch between AOI and average wavelength trends seems to be more related to the substantial increase of aerosol and, to a greater extent, of water vapour content during summer in Bolzano [10], following the typical annual cycle in the mid-latitudes [11]. Since the absorption of aerosol and water vapour occurs mainly at the IR region, the spectrum results in a shift towards blue wavelengths, as observed by other authors [1, 12].

4.3 Spectral effects on PV performance

The relation of modeled average wavelength and module performance is evaluated for four different thin-film technologies: single junction amorphous silicon (a-Si), micromorph silicon (a-Si/μc-Si), Cadmium Telluride (CdTe) and Copper Indium Gallium Selenide (CIGS). A polycrystalline silicon technology (pc-Si) is also considered as reference.

The data is previously filtered for the following conditions:

- angle of incidence (AOI) less than 50°, in order to avoid angle dependence due to mismatch of cosine behaviour of pyranometer glass dome with respect to flat module plane [2] and minimize incident angle reflection losses
- clear sky conditions (DtGHI < 0.20)
- Performance Ratio range given by $PR_{avg}\pm\sigma$, in order to sort out not homogeneous irradiance conditions that can occur between pyranometer and module due to mountain shading or clouds [13]

As a second step, a temperature correction of array efficiency, η, to 25°C (T_{STC}) is performed in order to minimize temperature effects, using the following expression [14]:

$$\eta_{STC} = \eta \frac{1}{[1+\gamma_{STC}(T_{cell}-T_{STC})]} \quad (1)$$

that is

$$\eta_{STC} = \eta \frac{1}{[1+\gamma_{STC}(T_{cell}-25)]} \quad (2)$$

where γ_{STC} is the temperature coefficient of power (%/°C) from datasheet. In this work, the module temperature is in turn calculated using the formula described in Skoplaki et al. [15]:

$$T_{cell} = T + (NOCT - T_{NOCT})\frac{G}{G_{NOCT}}\frac{h_{w,NOCT}}{h_w(v)}\left[1 - \frac{\eta_{STC}}{\tau\alpha}(1+\gamma_{STC}T_{STC})\right] \quad (3)$$

T ambient temperature (°C)
$NOCT$ Nominal Operating Cell Temperature, calculated under the conditions G=800 W/m^2, T=20°C, W=1 m/s, given by the manufacturer
T_{NOCT} temperature under NOCT conditions
G irradiance (W/m^2)
G_{NOCT} irradiance under NOCT conditions
$h_w(v)$ wind convection coefficient
$h_{w,NOCT}$ wind convection coefficient at NOCT conditions
η_{STC} efficiency under STC conditions, given by the manufacturer
τ transmittance of the cover system
α absorption coefficient of the cells
T_{STC} temperature under STC conditions

In particular, the wind convection coefficient is a linear function of local wind speed close to the module, v, given by [15]:

$$h_w(v) = 5.7 + 3.8v$$

while the product $\tau\alpha$ can be assumed as 0.9 [15]. Equation 3 has been demonstrated to better fit the measured values of module temperature at ABD test facility than just considering ambient temperature, because it takes into account the cooling effect of wind on module [16].

Finally, the efficiency is normalized to an efficiency value corresponding to Air Mass 1.5, calculated with a fit on the overall filtered and temperature-corrected points.

In Figure 5 the normalized efficiency is plotted against modeled average wavelength, for the 4 thin-film technologies and the reference polycrystalline. Points are grouped for different in-plane irradiance levels, around 600, 800 and 1000 W/m^2. A linear fit of all points is also displayed. In Table 1 the percentage of the absolute variation of efficiency in the range between 675 and 725 nm is reported for each technology, together with the Root Mean Square Error (RMSE).

In general, higher irradiance levels correspond to more "blue-shifted" solar spectra, while lower irradiance levels span a broader range. In any case, the slope of cloud points corresponding to different irradiance levels seems to be the same, thus justifying the linear interpolation (black line) of all points.

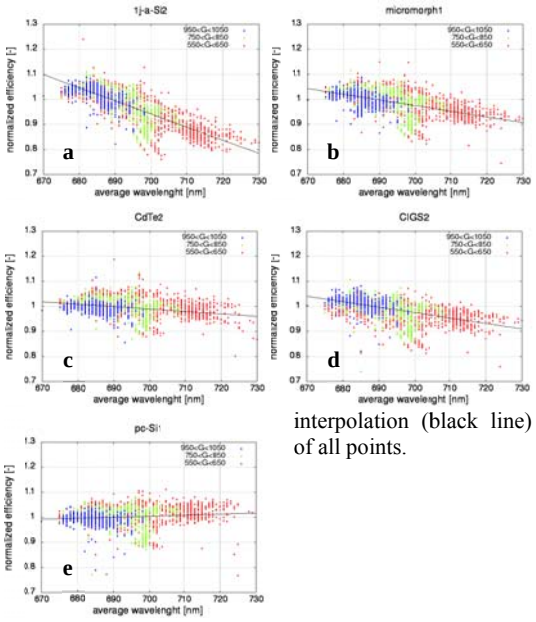

Figure 5: normalized efficiency against average wavelength, for clear sky conditions, angle of incidence less than 50°, sorted for shading and corrected to standard temperature of 25°C. Different in-plane irradiance levels (950<G<1050 W/m^2, 750<G<950 W/m^2, 550<G<650 W/m^2) are displayed, as well as the linear fitting curve (black line). a) a-Si, b) micromorph, c) CdTe, d) CIGS, e) pc-Si.

Table 1 absolute value of efficiency variation in the range 675-725 nm for the considered technologies, and root mean square error of the linear interpolation.

Module name	variation %	RMSE
1j-a-Si1	26.2	0.038
micromorph1	11.3	0.036
CdTe2	4.8	0.031
CIGS2	10.8	0.034
pc-Si1	2.1	0.035

In general, the efficiency of thin-film technologies, corrected for temperature, decreases at increasing wavelength of the solar spectrum. A direct correlation between these results and spectral responsivity (SR) of the considered technologies cannot be done due to the lack of SR measurements. These vary significantly between technologies, as well as between modules of same technology but different manufacturers [2]. Nevertheless, the behavior of thin-film technology seems to be in line with the results reported by different authors [1, 2]. In particular, the variation of efficiency is more evident in amorphous-silicon, where the effects of light-soaking and thermal annealing may play a certain role in addition to spectral effect. However, it has been demonstrated that this effects have a slightly lower influence than spectral effects [4] on module behaviour.

On the other hand, the polycrystalline silicon shows a different performance due to its efficiency that increases at higher wavelengths, as expected considering the typical higher spectral responsivity at near infrared (NIR) wavelengths.

By quantitatively knowing the spectral effects on different technologies is then possible to compare indoor with outdoor data, namely electrical parameters and temperature coefficients.

5 CONCLUSIONS

The average wavelength index calculated from modeled solar spectra with SPEMAGIC algorithm using satellite retrieved cloud information is used to spectrally characterize the Airport Bolzano Dolomiti (ABD) photovoltaic test installation site. Results show that the spectrum is shifted towards red wavelengths in presence of direct component of irradiance, and blue wavelengths in case of prevailing diffuse component due to cloud cover or mountain shading. The spectral content is in general related to air mass and angle of incidence, but also to aerosol and water vapour content of the atmosphere. In particular, their higher concentration during summer months results in a spectral shift towards lower wavelengths, thus giving a minimum level of average wavelength for the year.

The spectral effect of 4 different thin-film technologies and a polycrystalline silicon is also assessed through the relation between efficiency and average wavelength. Thin-films decrease their performance at increasing wavelengths. The efficiency variation in the range 675-725 nm results in 4.8% for CdTe, 10.8% for CIGS, 11.3% for micromorph, 26.2% for a-Si. The latter considerably higher value may be due to the addition of light-soaking and thermal annealing effects. The polycrystalline silicon shows the opposite trend, with increasing performance at increasing wavelengths. The efficiency variation results in 2.1% for this technology.

In general, the integral value of spectral irradiance calculated with SPECMAGIC shows a good agreement with the corresponding irradiance data measured at ABD, especially for the horizontal plane. A comparison between modeled and measured spectra will be also carried out in a future work in order to strengthen the consistency of this model.

6 ACKNOWLEDGMENTS

This work is financed through the project 2-1a-97 ”PV Initiative” in cooperation with the autonomous province of Bolzano-Alto Adige (GB, DM), through the Stiftung Suedtiroler Sparkasse (DM), and through the Interreg program IV Italy - Swiss by the European Funds for Regional Development (EFRE) (DM, JW, AT).

7 REFERENCES

[1] C. Cornaro, A. Andreotti, Influence of average photon energy index on solar irradiance characteristics and outdoor performance of photovoltaic modules, Progress in Photovoltaics: Research and Applications, 2012.

[2] M. Schweiger, M. Ulrich, I. Nixdorf, L. Rimmelspacher, U. Jahn, W. Herrmann, Spectral analysis of various thin-film modules using high precision spectral response data and solar spectral irradiance data, 27th European Solar Energy Conference and Exhibition, Frankfurt, 2012, 3284-3290.

[3] A. Virtuani, L. Fanni, Seasonal power fluctuations of amorphous silicon thin-film solar modules: distinguishing between different contributions, Progress in Photovoltaics: Research and Applications, 2012.

[4] R. Gottschalg, D.G. Infield, M.J. Kearney, Experimental study of variations of the solar spectrum of relevance to thin film solar cells, Solar Energy Materials and solar cells, Volume 79, September 2003, pp. 527-537.

[5] B. Marion, Influence of Atmospheric Variations on Photovoltaic Performance and Modeling Their Effects for Days with Clear Skies, 38th IEEE Photovoltaic Specialists Conference, Austin, June 2012.

[6] R. Mueller, T. Behrendt, A. Hammer, A. Kemper, A new algorithm for the satellite-based retrieval of solar surface irradiance in spectral bands, Remote Sensing, Volume 4, September 2012, pp. 622-647.

[7] S. Kato, T. Ackerman, J. Mather, E. Clothiaux, The k-distribution method and correlated-k approximation for a short-wave radiative transfer, Journal of Quantitative Spectroscopy and Radiative Transfer, Volume 62, 1999.

[8] Meteoswiss: CM SAF Data and Methods [Online]. Available at http://meteosuisse.ch/web/en/research/current_projects/climate/cmsaf/data_methods.html [Accessed: 26-Feb-2012].

[9] G. Belluardo, M. Pichler, D. Moser, M. Nikolaeva-Dimitrova, One-year comparison of different thin film technologies at Bolzano Airport Test Installation. Fuelling the Future: Advances in Science and Technologies for Energy Generation, Transmission and Storage, pp. 229-234.

[10] NASA: Aerosol Robotic Network (AERONET) [Online]. Available at http://aeronet.gsfc.nasa.gov/ [Accessed: 06-Sept-2013].

[11] J.P. Ortiz de Galisteo, Y. Bennouna, C. Toledano, V. Cachorro, P. Romero, M.I. Andrés, B. Torres, Analysis of the annual cycle of the precipitable water vapour over Spain from 10-year homogenized series of GPS data. Quarterly Journal of the Royal Meteorological Society, May 2013.

[12] M. Chegaar, P. Mialhe, Effect of atmospheric parameters on the silicon solar cells performance, Journal of Electron Devices, Volume 6, 2008, pp. 173-176.

[13] D. Moser, M. Pichler, M. Nikolaeva-Dimitrova, Filtering procedures for reliable outdoor temperature coefficients in different photovoltaic technologies, Journal of Solar Energy Engineering, Volume 136, August 2013.

[14] A. Colli, W.J. Zaaiman, Maximum-Power-Based PV Performance Validation Method: Application to single-Axis tracking and fixed-tilt c-Si systems in the Italian Alpine region, Progress in Photovoltaics: Research and Applications, Volume 4, October 2012, pp. 555-563.

[15] E. Skoplaki, A.G. Boudouvis, J.A. Palyvos, A simple correlation for the operating temperature of photovoltaic modules of arbitrary mounting, Solar Energy Materials & Solar Cells 92, 2008, pp. 1393-1402.

[16] C. Schwingshackl, M. Petitta, J. E. Wagner, G. Belluardo, D. Moser, M. Castelli, M. Zebisch, A. Tetzlaff, Wind effect on PV module temperature: analysis of different techniques for an accurate estimation, Energy Procedia, Vol. 40, 2013, pp. 77-86.